การสังเคราะห์ ศึกษาโครงสร้าง คุณสมบัติเชิงแสงผ่านปฏิกิริยาการระงับ และคุณสมบัติในการเป็นสารออกฤทธิ์ยับยั้งเซลล์มะเร็งของสารประกอบเชิงซ้อนเออริเดียม(III) กับลิแกนด์ triphenylphosphine (PPh_3)

Synthesis, Characterization, Photo-Physical Properties, Quenching Reaction and Anticancer Activity Against Cancer Cell Lines of Ir(III) Complex Containing PPh_3 Ligand

รัตตัญญู คงพันธุ์[1] เสาวนิต ทรายทอง[1] จวงจันทร์ วุฒิพันธุ์[1] อวิรุทธิ์ ชินกุลกิจนิวัฒน์[2] และ นรารักษ์ หลีสกุล[1*]
Rattanyu Kongpan[1], Saowanit Saithong[1], Juangjan Wuttipan[1], Avirut Chinkulkijniwat[2] and Nararak Leesakul[1*]
Received: 20 May 2022, Revised: 21 June 2022, Accepted: 27 June 2022

บทคัดย่อ

ในงานวิจัยนี้สังเคราะห์สารประกอบเชิงซ้อน $[Ir(ppy)_2(PPh_3)Cl].CH_2Cl_2.H_2O$ ผ่านปฏิกิริยาการแทนที่ระหว่างเออริเดียม(III)ไดเมอร์กับลิแกนด์ triphenylphosphine (PPh_3) ในตัวทำละลายไดคลอโรมีเทน ศึกษาโครงสร้างของสารประกอบเชิงซ้อนดังกล่าวด้วยเทคนิค Single crystal X-ray diffraction, ^{1}H-NMR, FTIR และการวิเคราะห์ปริมาณธาตุ ซึ่งพบว่าโครงสร้างของสารประกอบเชิงซ้อนชนิดนี้มีโครงสร้างเป็นทรงเหลี่ยมแปดหน้าบิดเบี้ยว (distorted octahedral) จากการศึกษาคุณสมบัติเชิงแสงของสารประกอบเชิงซ้อน $[Ir(ppy)_2(PPh_3)Cl].CH_2Cl_2.H_2O$ โดยใช้ความยาวคลื่นสำหรับการกระตุ้นอยู่ที่ 350 นาโนเมตร พบว่ามีการเปล่งแสงที่ 489 นาโนเมตร และสารประกอบเชิงซ้อนข้างต้นมีคุณสมบัติในการเป็นเซนเซอร์ตรวจวัดความเข้มข้นของเหล็กประจุ 3+ (Fe(III)) ในลักษณะที่เป็น turn-off luminescent นอกจากนี้ ผลการศึกษาความสามารถของสารประกอบเชิงซ้อน $[Ir(ppy)_2(PPh_3)Cl].CH_2Cl_2.H_2O$ ในการออกฤทธิ์ยับยั้งการเจริญเติบโตของเซลล์มะเร็งเต้านม 4 ชนิด ได้แก่ MCF-7, MDA-MB-231, MDA-MB-468 และ BT-549 พบว่าสามารถยับยั้งเซลล์มะเร็งเต้านมทั้ง 4 ชนิด โดยให้ค่า IC_{50} เท่ากับ 7.03±0.99, 5.85±0.36, 6.10±0.14 และ 6.20±0.07 μM ตามลำดับ

คำสำคัญ: สารประกอบเชิงซ้อนเออริเดียม(III), ไตรฟีนิลฟอสฟีน, การเปล่งแสง, ฤทธิ์ต้านมะเร็ง

---

[1] สาขาวิทยาศาสตร์กายภาพ คณะวิทยาศาสตร์ มหาวิทยาลัยสงขลานครินทร์ อำเภอหาดใหญ่ จังหวัดสงขลา 90110

[1] Division of Physical Science and Center of Excellence for Innovation in Chemistry, Faculty of Science, Prince of Songkla University, Hat Yai, Songkhla 90110, Thailand.

[2] สำนักวิชาวิศวกรรมศาสตร์ มหาวิทยาลัยเทคโนโลยีสุรนารี อำเภอเมือง จังหวัดนครราชสีมา 30000

[2] Center of Excellence in Civil Engineering, School of Civil Engineering, Suranaree University of Technology, Muang, Nakhon Ratchasima 30000, Thailand.

[*] Corresponding author, e-mail: nararak.le@psu.ac.th Tel: 0 74288421

ABSTRACT

In this study, $[Ir(ppy)_2(PPh_3)Cl].CH_2Cl_2.H_2O$ complex was synthesized via the substitution reaction between Ir(III) dimeric complex with triphenylphosphine (PPh_3) ligand in dichloromethane solvent. The complex was characterized by single crystal X-ray diffraction, ^{1}H-NMR, FTIR spectroscopies and elemental analysis. Photo-physical properties of the title complex were studied for a further application based on its luminescence at 489 nm with an excitation wavelength at 350 nm. It behaved as a turn-off luminescent chemosensor toward Fe(III) ion concentrations. In addition, it was investigated for anti-breast cancer activity against four cell lines of MCF-7, MDA-MB-231, MDA-MB-468 and BT-549 with IC_{50} values: 7.03±0.99, 5.85±0.36, 6.10±0.14 and 6.20±0.07 μM, respectively.

Key words: iridium (III) complex, triphenylphosphine, luminescence activity, anticancer

INTRODUCTION

Currently, Iridium (III) complexes have been widely explored for their photo-physical properties and biological activities (Liu and Sadler, 2014; Lu *et al*., 2015; Esteruelas *et al*., 2017). There are variety investigations on LEDs application due to the emissive luminescence intensities of Ir(III) complexes (Zanoni *et al*., 2015) Moreover, Iridium(III) complex-based chemo-sensors are also used *in vitro* and *in vivo* metal ions detection because of their photophysical properties, for example, large Stoke shift, high quantum yield, and long lifetime of luminescent emission (Ma *et al*., 2019). The cisplatin complex was recognized for a potent chemotherapeutic drug and cytotoxic effects on cancer cells treatment (Hao *et al.*, 2019; Brown *et al*., 2019). Many side effects of using cisplatin have affected the patients such as vomiting, hair fall, kidney toxic, and blood test abnormalities, etc. (Xie *et al*., 2020). Regarding these effects, Iridium(III) complexes have been widely studied for their cytotoxicity against various types of cancer cells because of the promising properties in iron mimicking, less toxic to normal cells and able to penetrate to cancer cells (Komarnicka *et al*., 2022; Chen *et al*., 2022). For example, the $[Ir(\eta^5k^1\text{-}C_5Me_4CH_2py)(2\text{-phenylpyridine})]PF_6$ complex where $C_4Me_4CH_2py$ is 2-((2,3,4,5-tetramethylcyclopenta-1,3-dien-1-yl)methyl)pyridine was studied in its cytotoxicity on A2780, colon tumor cell line (HCT 116) and MCF-7 breast cancer cell line. The results exhibited that complex showed higher growth inhibition potential than cisplatin for A2780, HCT116 and MCF7 (Conesa *et al*., 2020). Moreover, the synthesized iridium(III) hydride complex displayed good results for cytotoxicity studies of anticancer activities to A2780 and MCF7 cells with IC_{50} = 0.98 μM and 4.46 μM, respectively (Wang *et al*., 2019). In our previous work, we have reported the antiproliferative activity of cyclometalated $[Ir(ppy)_2(dppm)Cl]$ against 3 breast cancer cells (Leesakul *et al*., 2021). This complex displayed the greater response more than cisplatin for those 3 cell lines about 25-160 folds. Therefore, it is interesting to explore anticancer activity of cyclometated Ir(III) complex with other organophosphorus ancillary ligands comparison to the different medicinal drug for cancer treatment. In this present work, the $[Ir(ppy)_2(PPh_3)Cl].CH_2Cl_2.H_2O$ complex has been synthesized, characterized and studied for its cytotoxicity against 4 breast cancer cells; MCF-7, MDA-MB-231, MDA-MB-468 and BT-549; comparison with doxorubicin which is a chemotherapy medication for cancer treatment. Besides, many works have focused on chemo-sensor application (Liu *et al*., 2017; Ma *et al*., 2018). Most of them are ionic complexes of Ir(III) based 2-phenylpyridine derivatives. They have demonstrated to be both turn-on and turn-off luminescent probes (Ru *et al*., 2014; Ge *et al*., 2022). Nevertheless, there is very seldom to report for neutral complexes. Therefore, exploring the quenching reactions between the title complex with 6 transition metals and heavy metal ions (Fe^{3+}, Ni^{2+}, Cu^{2+}, Mn^{2+}, Co^{2+} and Pb^{2+}) has been our challenge.

MATERIALS AND METHODS

Materials

Chemicals were obtained from commercial sources and used without further purification. Iridium(III)chloride trihydrate, 2-phenylpyridine and Triphenylphosphine were purchased from Merck, Sigma-Aldrich and TCI, respectively. Dichloromethane, diethyl ether and *N*,*N*-dimethylformamide solvents were A.R. grade and were purchased from Labscan.

Instrumentation

^{1}H-NMR spectrum in $CDCl_3$ was obtained from 300 MHz of BRUKER ADVANCE 300 FT-NMR spectrometer. Vibrational frequencies of FTIR spectrum were measured by using Nicolet iS5 FTIR spectrophotometer in the range between 4000-400 cm^{-1}. The melting point of the $Ir(ppy)_2(PPh_3)Cl$ complex was determined by Thomas-Hoover, Unimelt. The temperatures were scanned between 0 to 360 ºC. Elemental analysis was performed using CHNS/O analyzer, Flash 2000, ThermoScientific, Italy.

Single crystal XRD pattern of $[Ir(ppy)_2(PPh_3)Cl].CH_2Cl_2.H_2O$ complex was collected by a D8 VENTURE Bruker AXS diffractometer with PHOTON II Charge-Integrating Pixel Array area detector using graphite-monochromated Mo K_α radiation (λ= 0.71073 Å).The diffraction pattern was monitored from 30304 reflections. The softwares SMART, SAINT v8.38A and SADABS were used to interpret the raw data. The structure was solved by SHELXS (Sheldrick, 2015). The anisotropic thermal parameters were refined for non-hydrogen atoms by the anisotropic thermal parameters. A riding model was utilized to refine calculations with all hydrogen atoms placed in ideal positions. The materials and molecular graphics for publication were prepared with the WinGX 2018/3 (Farrugia, 2012) and Mercury 2020.3 (Macrae *et al*., 2008) programs. Crystal data of $Ir(ppy)_2(PPh_3)Cl$ were deposited in the Cambridge Crystallographic Data Center and can be provided upon request, using the access CCDC code of: 2172804, via: http://www.ccdc.cam.ac.uk/data_request/cif (or from the Cambridge Crystallographic Data Centre, 12 Union Road, Cambridge CB21EZ, U.K.; fax: +44 1223 336 033 or email deposit@ccdc.cam.ac.uk). The X-ray data are given in the supplementary information.

Synthesis pathway of $[Ir(ppy)_2Cl]_2$ and $[Ir(ppy)_2(PPh_3)Cl].CH_2Cl_2.H_2O$ complex

Iridium dimer was a precursor for the substitution reaction of $[Ir(ppy)_2(PPh_3)Cl].CH_2Cl_2.H_2O$ complex synthesis. The dimer was synthesized by the reaction between iridium(III) chloride trihydrate and 2-phenylpyridine in 2-ethoxyethanol: distilled H_2O. A mixture of iridium(III) chloride trihydrate (0.1493 g, 0.5 mmol) and 2-phenylpyridine (0.2850 mL, 2 mmol) was refluxed in 2-ethoxyethanol: distilled H_2O = 3: 1 (30:10 mL) for 24 h under Ar gas. After cooling to room temperature, the mixture was filtered and washed with diethyl ether (Xu *et al*., 2011). The yellow powder of $[Ir(ppy)_2Cl]_2$ was collected and characterized.

Yield: 40.3 %, Melting point: 283-284 ºC, Anal. Cald (%) for IrC40H31 N2PCl: C 49.28, H 2.99, N 5.23. Found: C 48.41, H 2.96, N 4.94, FTIR (KBr, cm^{-1}) see Figure S1: νC-H 3058, νC-H 756, νC=C 1478, νC-N 1268, νC=N 1605, νIr-N 735, νIr-Cl 460. ^{1}H NMR (300 MHz, d_6-$CDCl_3$) see Figure S2: 9.23(4H, d, *J* = 5.1Hz, H8), 7.87 (4H, d, *J* = 7.8Hz, H4), 7.74 (4H, t, *J* = 7.80Hz, H3), 7.49 (4H, d, *J* = 7.8 Hz, H5), 6.76 (8H, m, *J* = 8.7Hz, H6/7), 6.56 (4H, t, *J* = 7.8Hz, H2), 5.93 (4H, d, *J* = 7.5Hz, H1).

The $[Ir(ppy)_2Cl]_2$ was used to further react with triphenylphosphine ligand in dichloromethane for synthesizing $[Ir(ppy)_2(PPh_3)Cl].CH_2Cl_2.H_2O$ complex. A solution of iridium(III) dimer (0.1635 g, 0.5 mmol) and triphenylphosphine (0.0787 g, 2 mmol) was refluxed in 30 mL of dichloromethane for 12 h under Ar atmosphere. The complex was filtered and washed by using diethyl ether for three times.

Yield: 48.3%, Melting point: 358-360 ºC, Anal. Cald (%) for Ir2C44H32N4Cl2: C 60.18, H 3.91, N 3.51. Found: C 60.88, H 3.97, N 3.54, FTIR see Figure 4: νsp^2 C-H 3000, νC=C 2345/1730, νC=N 1650, νC-N 1420, νC-C)1010, νC-H 800-1000, νIr-P780, νIr-N 760, νIr-Cl510 cm^{-1}. ^{1}H NMR (300 MHz, d_6-$CDCl_3$) see Figure 5: 9.24 (2H, d, *J* = 6.04

Hz, H1), 8.85 (2H, d, J = 4.92 Hz, H4), 7.86 (2H, d, J = 7.83 Hz, H5), 7.73 (2H, t, J = 14.76 Hz, H2), 7.5 (8H, m, H3/6/7/8), 6.84 (5H, m, H9/10/11).

Photo-physical properties

Absorption spectra of $[Ir(ppy)_2(PPh_3)Cl].CH_2Cl_2.H_2O$ complex in dichloromethane (CH_2Cl_2) were recorded by TU-1950 model UV-Visible Spectrophotometer. A standard quartz cell of 1x1 cm^2 was used. Deuterium and tungsten lamps were light sources in UV and visible regions, respectively.

Photoluminescence (PL) spectra were monitored by Cary Eclipse Fluorescence spectrometer, Agilent Technology. Relative quantum yield of $[Ir(ppy)_2(PPh_3)Cl].CH_2Cl_2.H_2O$ in CH_2Cl_2 was determined using Kotelevskiy equation (Kotelevskiy, 1998; Rosspeintner *et al*., 2006; Yoopensuk *et al.*, 2012) at 25 ^oC. Diluted concentrations of 5 μM of $[Ir(ppy)_2(PPh_3)Cl].CH_2Cl_2.H_2O$ sample and coumarin -6 reference standard were prepared in CH_2Cl_2 and ethanol, respectively. Absorbances of both solutions at 350 nm were less than 0.05 for preventing self-quenching reaction. The quantum yield of coumarin-6 in ethanol at 25 ^oC was 0.8 (Drexhage, 1976).

Photo-induced electron transfer between the $[Ir(ppy)_2(PPh_3)Cl].CH_2Cl_2.H_2O$ luminophore and metal ions was carried out using quenching experiments in dimethyl- formamide (DMF). Samples consisted of a steady concentration of 0.03 mM of the luminophore with various concentrations 0.05-0.65 mM of metal ions. Stern-Volmer plot was applied to determine the Stern-Volmer constant, while Job's plot was used to identify the stoichiometry of a binding between iridium(III) luminophore and selective metal ion. Benesi-Hildebrand was manipulated to calculate an apparent constant (K_{app}) of 1:1 binding.

Anticancer assay

The anti-breast cancer activity measurements were carried out using the MTT assay against MCF-7 (ATCC HTB-22), MDA-MB-231 (ATCC HTB-26), MDA-MB-468 (ATCC HTB-132) and BT-549(ATCC HTB-122) cell lines. The cytotoxicity of complex against breast cancer cells was evaluated and compared with doxorubicin as a positive control. IC_{50} values were reported.

RESULTS AND DISCUSSION

Synthesis and characterization

$[Ir(ppy)_2(PPh_3)Cl].CH_2Cl_2.H_2O$ complex was synthesized by the reaction of iridium (III) dimer with the P-donor ligand of triphenylphosphine in dichloromethane (Scheme 1).

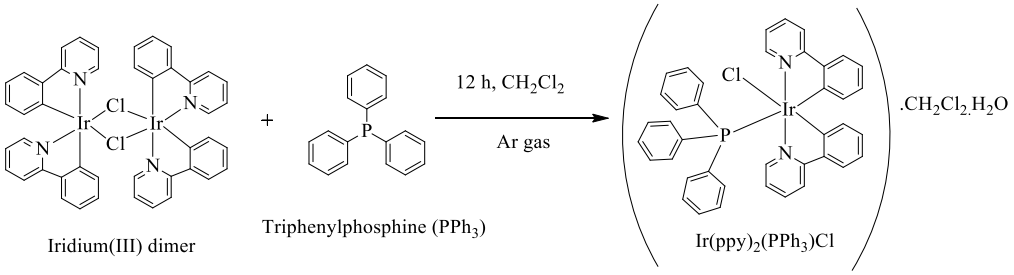

Scheme 1 Synthesis pathway $[Ir(ppy)_2(PPh_3)Cl].CH_2Cl_2.H_2O$ complex

In order to confirm the structure of studied complex, results from single crystal XRD, FTIR ^{1}H-NMR and elemental analysis techniques were investigated. The crystallographic data of the $[Ir(ppy)_2(PPh_3)Cl].CH_2Cl_2.H_2O$ complex are displayed in Table 1. The complex shows distorted octahedral geometry with two molecules of 2-phenylpyridine (ppy) ligand, single molecule of triphenylphosphine and one Cl^- ligand (Figure 1). The $C_{pyridine}$ of these two rings are in *cis* orientation, while $N_{pyridine}$ are in *trans* position. Selected bond lengths and bond angles of this complex are shown in Table 2. Bond lengths of Ir-C (C22 and C11), Ir-N (N1 and N2), Ir-Cl and Ir-P are 2.026(11), 2.025(12), 2.048(10), 2.078(9), 2.493(3) and 2.410(3) Å, respectively, corresponding to the related structure reported by (Orpen *et*

al.,2006; Wang *et al*., 2005; Liu *et al*., 2009). Bond angles of coordination around iridium(III) ion deviate from 90 º and 180 º. The angles of C11-Ir1-N1 and C22-Ir1-N2 are 80.6(5) º and 80.5(5) °, respectively. It is very slightly different from related literatures; C29-Ir1-N1 and C40-Ir1-N2 are 80.5(3) º and 79.9(3) ° for $[Ir(ppy)_2(PPh_3)Cl].CH_2Cl_2.H_2O$ and 80.81(9) º in $[IrH\{\kappa^3\text{-}C,N,(C{-}H)(C_6H_4\text{-}py\text{-}Ph)\}(P^iPr_3)_2]BF_4$ (Castro-Rodrigo *et al*., 2019). The N1-Ir1-P1 and N2-Ir1-P1 are 89.0(3) º and 99.2(3) º, respectively similar to the report from Wang and co-worker (Wang *et al*., 2005). For C22-Ir1-Cl1, C1-Ir1-P17 and N1-Ir1-N2 angles are in between 169.7-174.4 º, respectively which deviates from ideal 180 º. Intramolecular π-π stacking between pyridine (C12-C16) and a phenyl ring of phosphine molecule (C23-C26), *Cg4···Cg7* = 3.674 Å and C-H···π of C40-H40···*Cg6*= 2.833 Å are observed (Figure 2). Moreover, two weak intramolecular H-bond interaction *viz*. C12-H12···Cl1 = 3.349(15) Å and C30-H30···Cl1 = 3.279(12) Å are monitored. For intermolecular interactions, H-bonds of C41-H41A···Cl1 = 3.74(2), O1-H1A···O1 = 3.08(15) and O1-H1B···O1 = 3.08(15) Å are found. In addition, C-H···π of C8-H8···*Cg8* = 2.988 Å are also detected (Figure 3).

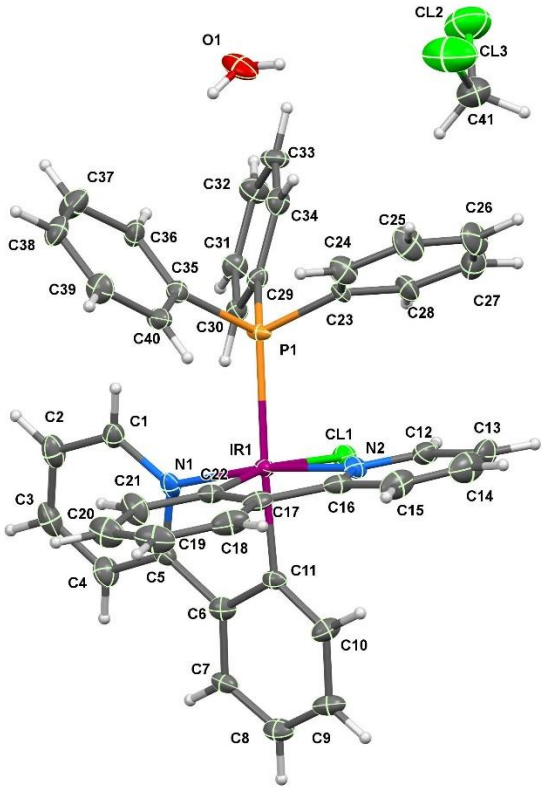

Figure 1 An ORTEP structure of the $[Ir(ppy)_2(PPh_3)Cl].CH_2Cl_2.H_2O$ complex with numbered

Table 1 Crystallographic data of the $[Ir(ppy)_2(PPh_3)Cl].CH_2Cl_2.H_2O$ complex

Empirical formula	$C_{40}H_{31}ClIrN_2P$, CH_2Cl_2, H_2O
Formula weight	901.23
Wavelength	0.71073 Å
Crystal system	Monoclinic
Space group	$P2_1/C$
Unit cell dimensions	a= 10.0757(10) Å
	b= 15.0507(13) Å
	c= 24.640(2) Å
	α= 90 º
	β = 99.570(4) º
	γ= 90 º
Temperature	296(2) K
Z	4
Density (calculated)	1.625 Mg/m^3
Absorption coefficient	3.920 mm^{-1}
Volume	3684.6(6) $Å^3$
Goodness-of-fit on F^2	1.107
Final R indices [$I>2\sigma(I)$]	$R1$= 0.0663
	wR2= 0.1664
R indices (all data)	$R1$= 0.0682
	wR2= 0.1679

Table 2 Selected bond lengths (Å) and angle (º) for the $[Ir(ppy)_2(PPh_3)Cl].CH_2Cl_2.H_2O$ complex

	Lengths		
Ir(1)-N(1)	2.048(10)	Ir(1) -Cl(1)	2.493(3)
Ir(1)-N(2)	2.078(9)	Ir(1) -C(22)	2.026(12)
Ir(1)-P(1)	2.410(3)	Ir(1) -C(11)	2.025(12)
	Angles		
C(22)-Ir(1)-C(11)	87.0(4)	N(1)-Ir(1)-P(1)	89.0(3)
C(22)-Ir(1)-N(1)	93.1(4)	N(2)-Ir(1)-P(1)	99.2(3)
C(11)-Ir(1)-N(1)	80.6(5)	C(22)-Ir(1)-Cl(1)	169.7(3)
C(22)-Ir(1)-N(2)	80.5(5)	C(11)-Ir(1)-Cl(1)	84.3(3)
C(11)-Ir(1)-N(1)	91.7(4)	N(1)-Ir(1)-Cl(1)	91.1(3)
N(1)-Ir(1)-N(2)	170.3(4)	N(2)-Ir(1)-Cl(1)	94.1(3)
C(22)-Ir(1)-P(1)	98.5(3)	P(1)-Ir(1)-Cl(1)	90.12(9)
C(11)-Ir(1)-P(1)	174.4(3)		

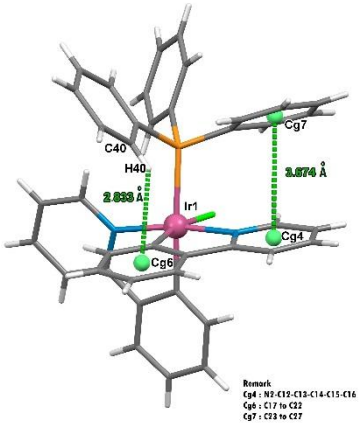

Figure 2 Intramolecular interactions of [Ir(ppy)$_2$(PPh$_3$)Cl].CH$_2$Cl$_2$.H$_2$O complex

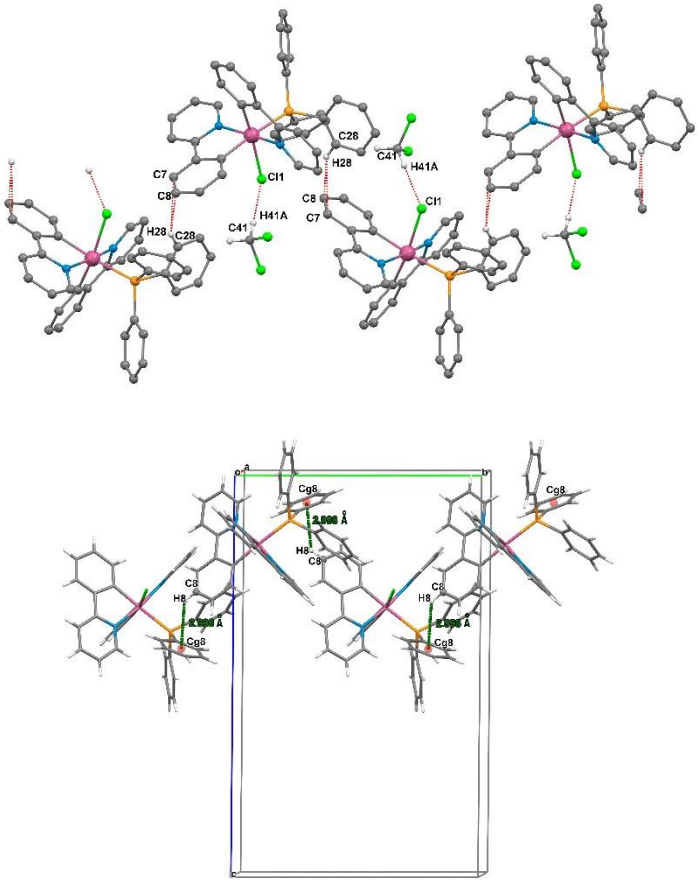

Figure 3 Intermolecular interactions of [Ir(ppy)$_2$(PPh$_3$)Cl].CH$_2$Cl$_2$.H$_2$O complex

Table 3 Hydrogen bonds for [Ir(ppy)$_2$(PPh$_3$)Cl].CH$_2$Cl$_2$.H$_2$O complex [Å and º].

D-H...A	d(D-H)	d(H...A)	d(D...A)	<(DHA)
C(12)-H(12)...Cl(1)	0.93	2.70	3.349(15)	127.8
C(41)-H(41A)...Cl(1)#1	0.97	2.77	3.74(2)	173.8
C(30)-H(30)...Cl(1)	0.93	2.79	3.279(12)	113.8
O(1)-H(1A)...O(1)#2	1.07(16)	2.51(14)	3.08(15)	113(10)
O(1)-H(1B)...O(1)#2	0.86(4)	2.59(12)	3.08(15)	117(11)

Symmetry transformations used to generate equivalent atoms: #1 -x, y+1/2,-z+1/2 #2 -x+1,-y+2,-z+1

FTIR spectrum (Figure 4) of the $[Ir(ppy)_2(PPh_3)Cl].CH_2Cl_2.H_2O$ complex exhibited characteristic peaks during 1650-450 cm^{-1} range. The vibrational frequencies of the coordination between iridium(III) metal center and donating atoms of N(ppy), P(PPh_3) and Cl were found at 698, 736 and 522 cm^{-1}, respectively. ^{1}H-NMR spectrum (Figure 5) of $[Ir(ppy)_2(PPh_3)Cl].CH_2Cl_2.H_2O$ complex was measured in $CDCl_3$. The coupling signals presented the chemical shift mainly in 6.5-9.5 ppm range corresponding to numbers of protons of pyridine rings from ppy ligand and phenyl rings from PPh_3 ligand.

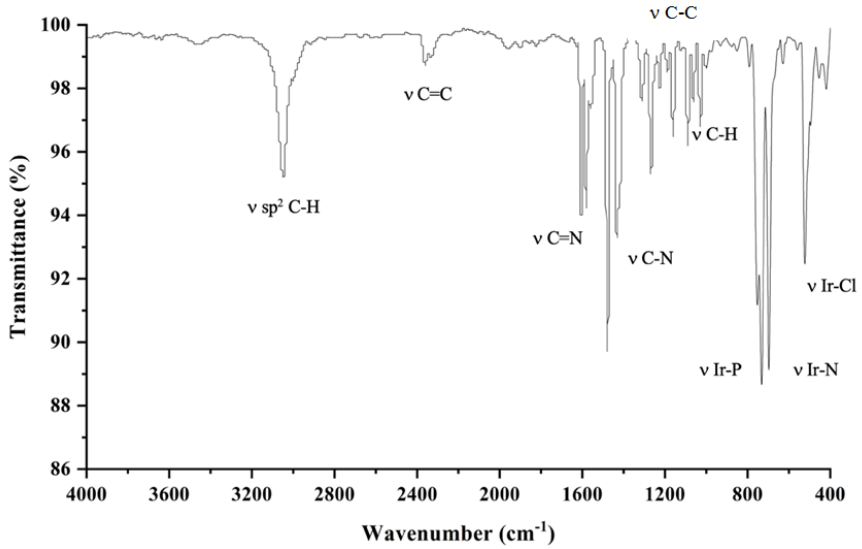

Figure 4 FTIR spectrum of $[Ir(ppy)_2(PPh_3)Cl].CH_2Cl_2.H_2O$ complex

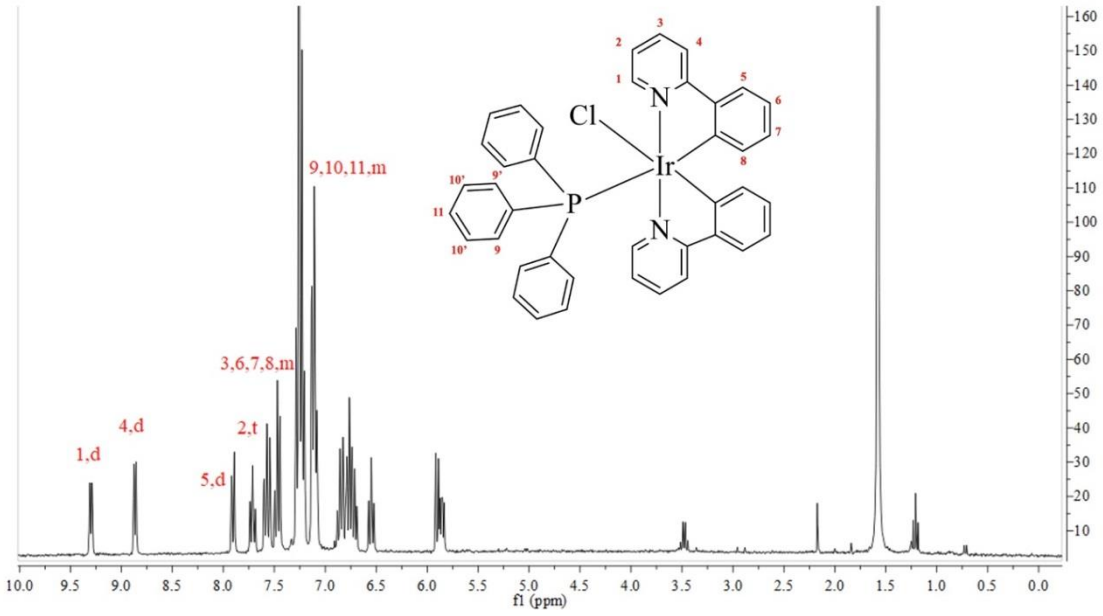

Figure 5 ^{1}H-NMR spectrum of $[Ir(ppy)_2(PPh_3)Cl].CH_2Cl_2.H_2O$ complex

Photo-physical properties and quenching reaction

The UV-Visible spectrophotometer was used to study the electronic spectra of complex. Absorption spectrum of 0.2 mM of $[Ir(ppy)_2(PPh_3)Cl].CH_2Cl_2.H_2O$ dimethylformamide (DMF) solution was measured. The absorption spectrum of the Iridium(III) complex showed an absorption band at λ_{max} 388 nm (Figure 6)

with molar extinction coefficient (ε) of 1781 $M^{-1}cm^{-1}$ defined the transition from charge transfers (CTs) transition in the complex (Leesakul *et al*., 2021). The emission spectrum of $[Ir(ppy)_2(PPh_3)Cl].CH_2Cl_2.H_2O$ displayed a luminescent band at 489 nm and a shoulder at 525 nm when excited at 350 nm (Figure 6) in dimethylformamide (DMF) solvent.

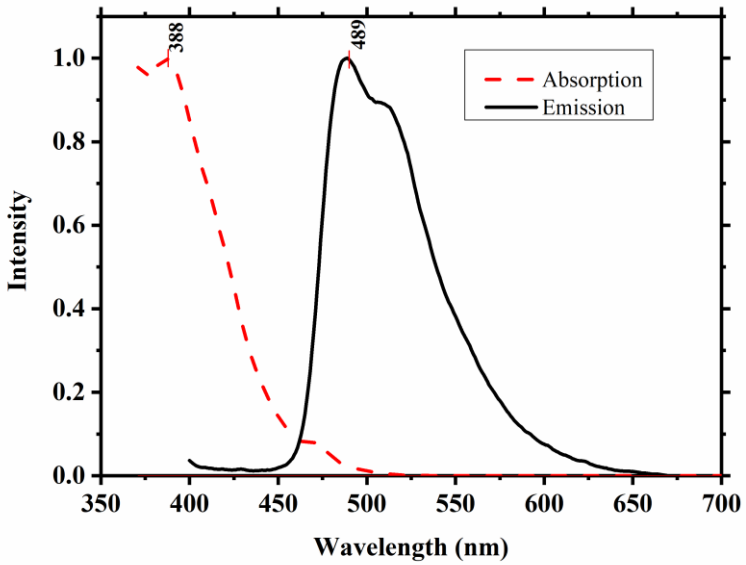

Figure 6 Absorption and emission spectra of $[Ir(ppy)_2(PPh_3)Cl].CH_2Cl_2.H_2O$ in DMF

Quenching reaction between $[Ir(ppy)_2(PPh_3)Cl].CH_2Cl_2.H_2O$ complex and various metal ions (Fe^{3+}, Ni^{2+}, Cu^{2+}, Mn^{2+}, Co^{2+} and Pb^{2+}) were investigated in DMF with the concentration range of $5x10^{-5}$ to $6.5x10^{-4}$ M. It was found that the Ir(III) complex was selective to Fe(III) as shown in Figure 7. The luminescence intensities of $[Ir(ppy)_2(PPh_3)Cl].CH_2Cl_2.H_2O$ complex gradually decreased corresponding to the increasing concentrations of Fe(III) solution, while others did not obviously show the quenching behavior (Figure 8). In addition, the interfering tests of Ir(III) with a presence of Fe(III) and other metal ions, as shown in Figure 8, were studied through recording the luminescence quenching ratio on Fe(III) with the addition of other interfering metal ions. It was found that all other metal ions did not interfere with the detection of Fe(III). The presence of Fe(III) enormously quenched the luminescence of our studied complex. Quenching efficiency was above 95 % with 0.2 mM of Ir(III) complex and the detection limit (DL) was 18.4 µM. Stern-Volmer plot was used to determine the Stern-Volmer constant (K_{SV}) which tells how good of electron transfer from Ir(III) to Fe(III). This plot is a relative between I_0/I (y-axis) versus [Q] (x-axis) where $I_0$is the intensity of Ir(III) without quencher, it is the intensity of Ir(III) with presence of each concentration of Fe(III) solution, and [Q] is the concentration of quencher. The SV plot showed a non-linear with a curve bending upward to the y-axis (Figure 9) which can occur either from ground state complex formation or inner filter effect (Leesakul *et al*., 2017). Nevertheless, the K_{SV} can be determined from the linear plot up to 2.0×10^{-4} M of the concentration of Fe(III) (inset of Figure 9). Regarding Stern-Volmer equation, $I_0/I = K_{SV}.[Q]$, observed K_{SV} was 9330.26 M^{-1}.

To determine the stoichiometry of binding between the Ir(III) and Fe(III), Job plot was studied. There are in general three normal methods studying for complex ions: the method of continuous variations (Job's method), the mole-ratio methods, and the slope-ratio method (Harvey, 2013). It is one of the popular methods for ions in solution which indicates whether the formation is a 1:1 complex or not. The Job plot corresponds

to the mole fraction of the Fe(III) bound to the Ir(III) complex. Job plot for recent work is presented in Figure 10. For this graph, the maximum in the curve is the plot exhibited the maximum crossing point at $\chi = 0.5$. It revealed a 1:1 metal ion to complex binding stoichiometry.

In order to identify a binding constant (K_b) from the quenching reaction, modified Benesi-Hildebrand equation (1) was applied. This constant shows how good Fe(III) and Ir(III) complex are bound together. The parameter I_0 is initial fluorescence intensity of complex without quencher; I_c is fluorescence intensity of quencher bounded with complex; I is fluorescence intensity of complex in each concentration of quencher; and [Q] is concentration of metal ion.

$$\frac{1}{I_0 - I} = \frac{1}{I_0 - I_c} + \frac{1}{(I_0 - I_c)[Q]\,K_b} \qquad (1)$$

Benesi-Hildebrand plot (Figure 11) indicated the formation of a 1:1 complex (linear plot). With present study, the binding constant was 8.41×10^3 M^{-1} indicating high binding affinity between Ir(III) complex and Fe(III).

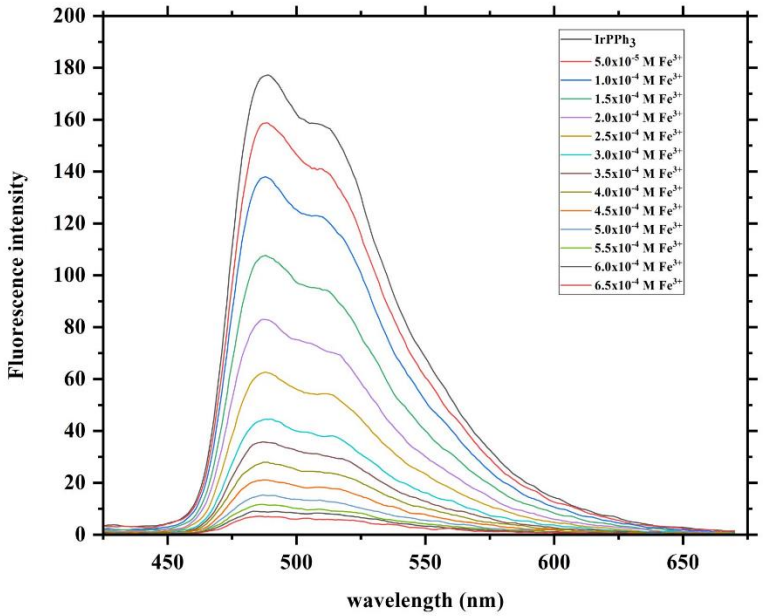

Figure 7 Quenching reaction between $[Ir(ppy)_2(PPh_3)Cl].CH_2Cl_2.H_2O$ and various concentrations of Fe(III) (5×10^{-5} to 6.5×10^{-4} M) in DMF

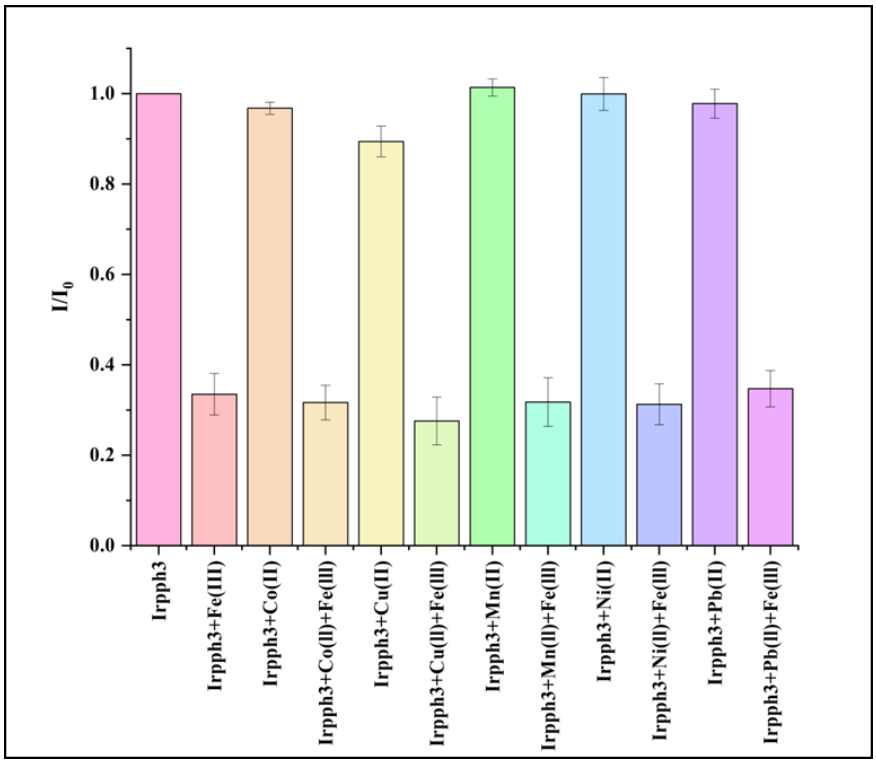

Figure 8 Luminescence spectra bar graph representation of $[Ir(ppy)_2(PPh_3)Cl].CH_2Cl_2.H_2O$ complex solution upon addition of various metal cations.

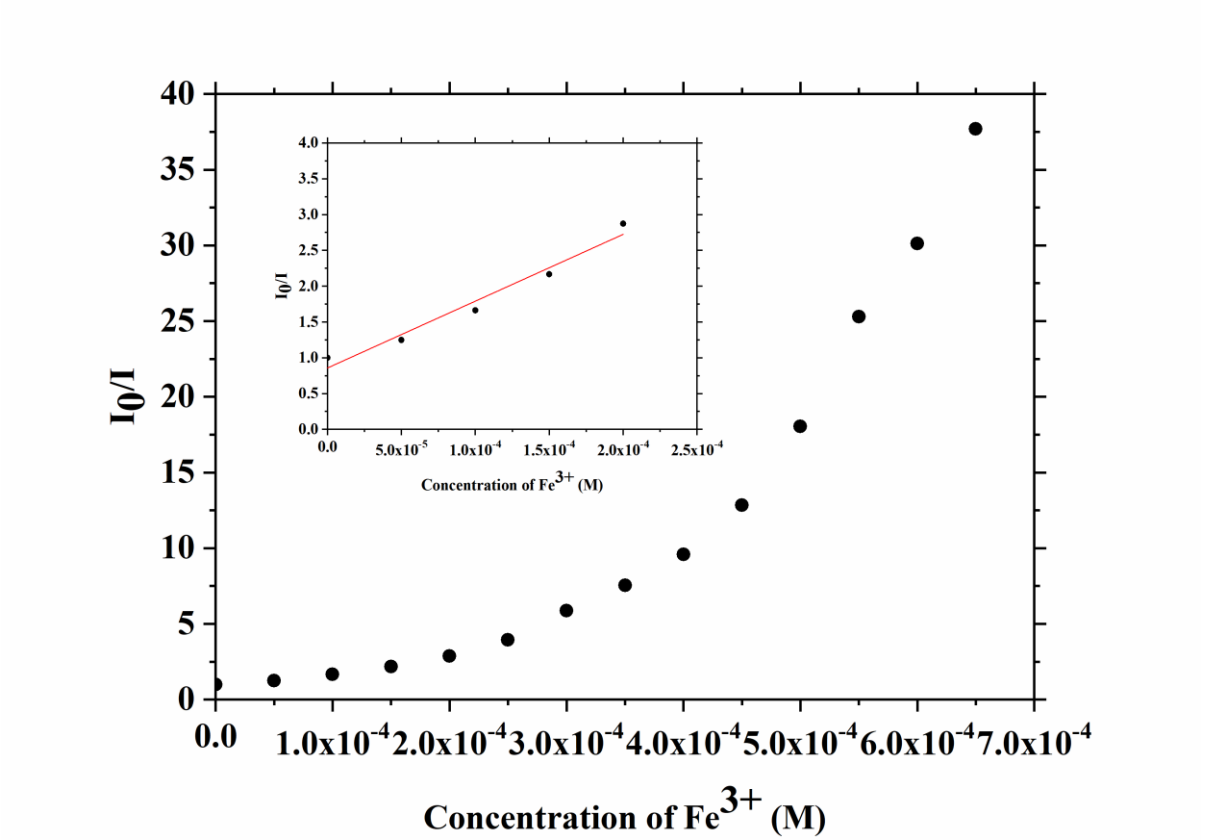

Figure 9 Stern-Volmer plot from quenching reaction between $[Ir(ppy)_2(PPh_3)Cl].CH_2Cl_2.H_2O$ and various concentrations of Fe(III)

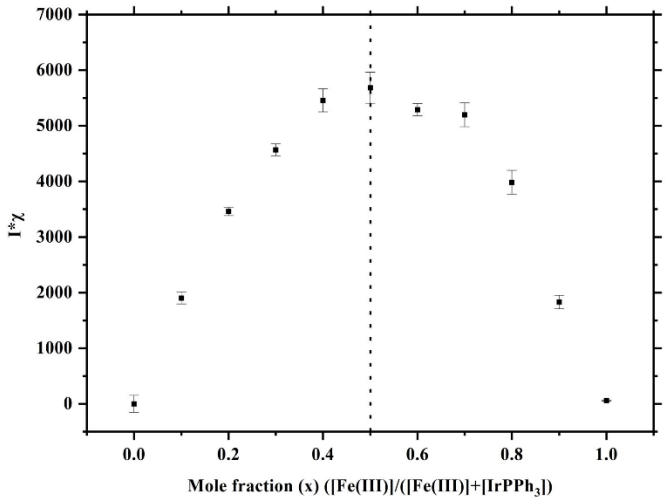

Figure 10 Job's plot (mole fraction) for determining the stoichiometry of the complex between $[Ir(ppy)_2(PPh_3)Cl].CH_2Cl_2.H_2O$ and Fe(III).

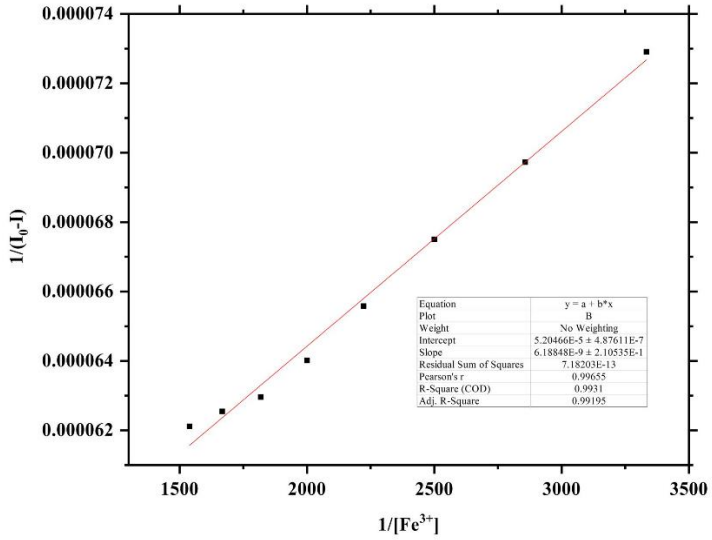

Figure 11 Benesi-Hidebrand plot of Fe(III) luminescence titration between $[Ir(ppy)_2(PPh_3)Cl].CH_2Cl_2.H_2O$ and various concentrations of Fe(III)

Anticancer properties

The anticancer activity of $[Ir(ppy)_2(PPh_3)Cl].CH_2Cl_2.H_2O$ complex was studied by MTT assay against human breast cancer cell lines such as MCF-7, MDA-MB-231, MDA-MB-468 and BT-549. The IC_{50} values were determined as shown in Table 3. The $[Ir(ppy)_2(PPh_3)Cl].CH_2Cl_2.H_2O$ complex is able to inhibit breast cancer cell line growth with IC_{50} values 7.03±0.99, 5.85±0.36, 6.10±0.14 and 6.20±0.07 μM for MCF-7, MDA-MB-231, MDA-MB-468 and BT-549 cell lines, respectively. Notably, the growth inhibition of MDA-MB-231 cell line presented the lowest IC_{50} value. Nevertheless, the IC_{50} values were all higher than those tested with Doxorubicin, an effective anticancer drug.

Table 3 IC_{50} values (μM) in various breast cancer cell lines after treatment with $[Ir(ppy)_2(PPh_3)Cl]$ complex for 48 h

Complexes	IC_{50} (μM)			
	MCF-7	**MDA-MB-231**	**MDA-MB-468**	**BT-549**
$[Ir(ppy)_2(PPh_3)Cl].CH_2Cl_2.H_2O$	7.03 ± 0.99	5.85 ± 0.36	6.10± 0.14	6.20± 0.07
Doxorubicin	1.20 ± 0.11	1.27 ± 0.02	1.14 ± 0.01	0.88 ± 0.05

CONCLUSION

The $[Ir(ppy)_2(PPh_3)Cl].CH_2Cl_2.H_2O$ complex was characterized by single crystal X-ray diffraction, elemental analysis and spectroscopic techniques. This study summarizes that the distorted Ir(III) complex adopted distorted octahedral geometry. The complex is a photoactive agent giving a large luminescence band between 450-650 nm. A significant turn -off luminescence against Fe(III) is observed when Fe(III) concentration increased. Owing to Job's plot and modified Benesi-Hildebrand, 1:1 ratio binding between the studied complex and Fe(III) is presented. Moreover, the complex possesses good cytotoxic activity against four breast cancer cells, but less than Doxorubicin for 5-7 times

ACKNOWLEDGMENTS

We would like to thank to *Science Achievement Scholarship of Thailand*, SAST for financial support for graduate study and research budget for Master Degree study for Ms.Rattanyu Kongpan. NL is grateful for partial financial support under contract number SCI64020775 from Prince of Songkla University and facility from Division of Physical Science, Faculty of Science, Prince of Songkla University. Authors would like thank Ms.Jutamat Hemtanon and Ms.Yasamin Manraden for their preliminary work on Ir(III) complex with PPh_3 ligand.

REFERENCES

Brown, A., Kumar, S. and Tchounwou, P.B. 2019. Cisplatin-Based Chemotherapy of Human Cancers. **Journal of Cancer Science & Therapy** 11(4): 97.

Castro-Rodrigo, R., Esteruelas, M.G., Gómez-Bautista, D., Lezáun, V., López, A.M., Oliván, M. and Oñate, E. 2019. Influence of the Bite Angle of Dianionic C,N,C-Pincer Ligands on the Chemical and Photophysical Properties of Iridium(III) and Osmium(IV) Hydride Complexes. **Organometallics** 38(19): 3707-3718.

Chen, W., Cai, X., Sun, Q., Guo, X., Liang, C., Tang, H., Huang, H., Luo, H., Chen, L. and Chen, J. 2022. Design and synthesis of aptamer-cyclometalated iridium(III) complex conjugate targeting cancer cells. **European Journal of Medicinal Chemistry** 236(1): 114335.

Conesa, J.J., Carrasco, A.C., Rodríguez-Fanjul, V., Yang, Y., Carrascosa, J.L., Cloetens, P., Pereiro, A. and Pizarro, A.M. 2020. Unambiguous Intra-cellular Localization and Quantification of a Potent Iridium Anticancer Compound by Correlative 3D Cryo X-Ray Imaging. **Angewandte Chemie International Edition** 59(3): 1270-1278.

Drexhage, K.H. 1976. Fluorescence Efficiency of Laser Dyes. **Journal of Research of the National Bureau of Standards. Section A, Physics and Chemistry** 80A(3): 421-428.

Esteruelas, M.A., Oñate, E. and Palacios, A.U. 2017. Identification of an iridium(III) complex with anti-bacterial and anti-cancer activity. **Journal of Organometallic Chemistry** 36(9): 1743-1755.

Farrugia, L.J. 2012. *WinGX* and *ORTEP for Windows*: an update. **Journal of Applied Crystallography** 45(4): 849 -854.

Ge, Z., Tong, X., Huang, Y., Li, W., Li, H., Lu, A. and Li, T. 2022. Highly Luminescent Dinuclear Iridium(III) Complexes Containing Phenan throline -Based Neutral Ligands as Chemosensors for Cu^{2+} Ion. **Organometallics** 41(6): 706-715.

Hao, H., Liu, X., Ge, X., Zhao, Y., Tian, X., Ren, T., Wang, Y., Zhao, C. and Liu, Z. 2019. Half-sandwich iridium(III) complexes with α-picolinic acid frameworks and antitumor applications. **Journal of Inorganic Biochemistry** 192(1): 52-61.

Harvey, D. 2013. **Spectrophotometric Studies of Complex Ions.** Chemistry LibreTexts. Available Source: https://chem.libretexts.org/Courses/Providence_College/CHM_331_ dvanced_Analytical _ Chemistry_1, June 29, 2020.

Komarnicka, U.K., Niorettini, A., Kozieł, S., Pucelik, B., Barzowska, A., Wojtala, D., Ziółkowska, A., Lesiów, M., Kyzioł, A., Caramori, S., Porchia, M. and Bieńko, A. 2022. Two out of Three Musketeers Fight against Cancer: Synthesis, Physicochemical, and Biological Properties of Phosphino Cu ^{I}, Ru ^{II}, Ir ^{III} Complexes. **Pharmaceuticals (Basel, Switzerland)** 15(2): 169.

Kotelevskiy, S.I. 1998. The true refractive index correction to the fluorescence intensity in the commercial fluorescence spectrophotometer. **Journal of Luminescence** 79(3): 211-214.

Leesakul, N., Kullawanichaiyanan, K., Mutić, S., Guzsvány, V., Nhukeaw, T., Ratanaphan, A., Saithong, S., Konno, T., Sirimahachai, U. and Promarak, V. 2021. A photoactive iridium(III) complex with 3-methyl-2-phenyl pyridine and 1,1-bis (diphenylphosphino) methane: Synthesis, structural characterization and cytotoxicity in breast cancer cells. **Journal of Coordination Chemistry** 74(14): 2380-2394.

Leesakul, N., Masen, D. and Grampp, G. 2017. Fluorescence Quenching Reaction of Chlorophyll a by Tris(acetylacetonate) iron(III) in Various Solvents. **Sains Malaysiana** 46(9): 1369-1377.

Liu, Z., Bian, Z. and Huang, C. 2009. Luminescent Iridium Complexes and Their Applications, pp. 113-142. *In* Bozec, H. and Guerchais, V., eds. **Molecular Organometallic Materials for Optics.** Springer Berlin, Heidelberg.

Liu, Z. and Sadler, P.J. 2014. Organo-iridium Complexes: Anticancer Agents and Catalysts. **Accounts of Chemical Research** 47(4): 1174-1185.

Liu, J., Wang, W., Li, G., Wang, R., Leung, C. and Ma, D. 2017. Luminescent Iridium(III) Chemo- sensor for Tandem Detection of F^{-} and Al^{3+}. **ACS Omega** 2(12): 9150-9155.

Lu, L., Lui, L., Chao, W., Zhong, H., Wang, M., Chen, X., Lu, J., Li, R., Ma, D. and Leung, C. 2015. Identification of an iridium(III) complex with anti -bacterial and anti-cancer activity. **Scientific Reports** 5(1): 14544.

Ma, D., NG, H., Wong, S., Vellaisamy, K., Wu, K. and Leung, C. 2018. Iridium(III) complexes as reaction based chemosensors for medical diagnostics. **Dalton Transactions** 47(43): 15278-15282.

Ma, D., Wong, S., Kang, T., Ng, H., Han, Q. and Leung, C. 2019. Iridium(III)-based chemosensors for the detection of metal ions. **Methods** 168(1): 3-17.

Macrae, C.F., Bruno, I.J., Chisholm, J.A., Edgington, P.R., McCabe, P., Pidcock, E., Rodriguez-Monge, L., Taylor, R., Van De Streek, J. and Wood, P.A. 2008. *Mercury CSD 2.0* - new features for the visualization and investigation of crystal structures. **Journal of Applied Crystallography** 41(2): 466-470.

Orpen, A.G., Brammer, L., Allen, F.H., Kennard, O., Watson, D.G. and Taylor, R. 2006. **Typical Interatomic Distances in Organic Compounds and Organometallic Compounds and Coordination Complexes of the d- and f-block metals.** Wiley, New York.

Rosspeintner, A., Angulo, G., Weiglhofer, M., Landgraf, S. and Grampp, G. 2006. Photophysical properties of 2,6-dicyano-N,N,N′,N′-tetramethyl-p-phenylenediamine. **Journal of Photochemistry and Photobiology A: Chemistry** 183(1): 225-235.

Ru, J., Guan, L., Tang, X., Dou, W., Yao, X., Chen, W., Liu, Y., Zhang, G., Liu, W., Meng, Y. and Wang, C. 2014. Turn-on Phosphorescent Chemodosimeter for

Hg^{2+} Based on a Cyclometalated Ir(III) Complex and Its Application in Time-Resolved Luminescence Assays and Live Cell Imaging. **Inorganic chemistry** 53(21): 11498-11506.

Sheldrick, G.M. 2015. Crystal structure refinement with SHELXL. **Acta Crystallographica Section C** 71(1): 3-8.

Wang, Y., Tang, A., Wang, Y., Xu, X. and Teng, F. 2005.Chlorobis[2-(2-pyridyl) phenyl-κ2N,C1](triphenylphosphine-κP) iridium(III) dichloromethane sesquisolvate. **Acta Crystallographica Section E** 61(4): 778-780.

Wang, X., Zhang, J., Zhao, X., Wei, W. and Zhao, J. 2019. Imaging and proteomic study of a clickable iridium complex. **Metallomics** 11(8): 1344-1352.

Xie, Y., Zhang, S., Ge, X., Ma, W., He, X., Zhao, Y., Ye, J., Zhang, H., Wang, A. and Liu, Z. 2020. Lysosomal-targeted anticancer half-sandwich iridium(III) complexes modified with lonidamine amide derivatives. **Applied Organometallic Chemistry** 34(5): e5589.

Xu, M., Zhou, R., Che, G., Wang, G., Wang, Z. and Xiao, Q. 2011. Synthesis and characterization of blue phosphorescent cyclometalated Ir(III) complexes containing 2-(imidazol-2-yl)pyridine as ancillary ligand. **Journal of Luminescence** 131(5): 909-914.

Yoopensuk, S., Tongying, P., Hansongnern, K., Pakawatchai, C., Saithong, S., Tantirungrotechai, Y. and Leesakul, N. 2012. Photoactive azoimine dyes: 4-(2-Pyridylazo)-*N*,*N*-diethylaniline and 4-(2-pyridylazo)-*N*,*N*-dimethylaniline: Computational and experimental investigation. **Spectrochimica Acta Part A: Molecular and Biomolecular Spectroscopy** 86(1): 538-546.

Zanoni, K., Coppo, P., Amaral, R. and Iha, N. 2015. Ir(III) complexes designed for light-emitting devices: beyond the luminescence color array. **Dalton Transactions** 44(33): 14559-14573.